Cell Reports, Volume *17*

Supplemental Information

Structural Dynamics of the YidC:Ribosome Complex during Membrane Protein Biogenesis

Alexej Kedrov, Stephan Wickles, Alvaro H. Crevenna, Eli O. van der Sluis, Robert Buschauer, Otto Berninghausen, Don C. Lamb, and Roland Beckmann

Supplemental Figures

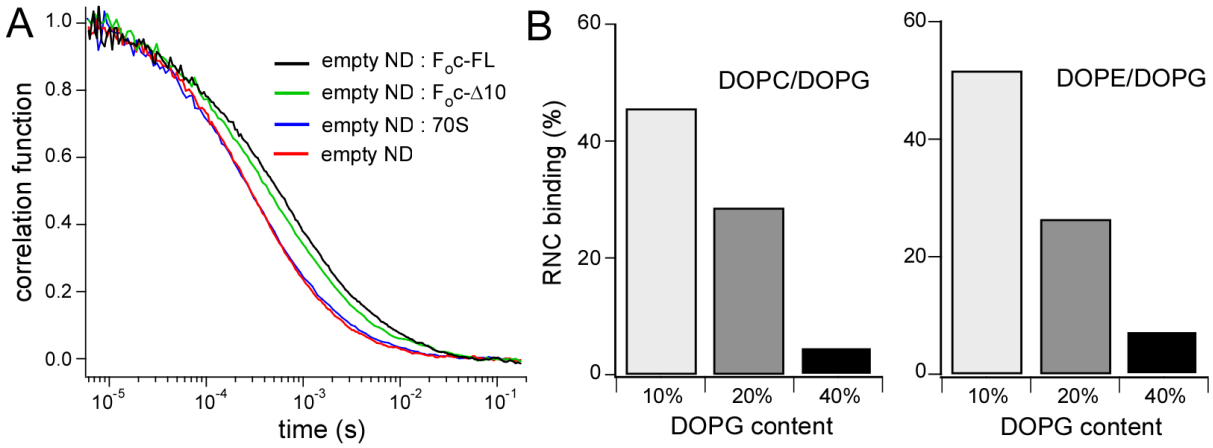

Figure S1. Related to the Figure 2. Spontaneous membrane insertion of F_oc depends on the lipid composition. Spontaneous insertion of hydrophobic nascent chains in the lipid bilayer is a potential pathway occurring in parallel to YidC-mediated insertion. (A) Auto-correlation curves of empty, YidC-free, nanodiscs (98% DOPC, 2% DOPE-Atto 488) diffusing in absence and presence of 200 nM RNC F_oc. The slower diffusion of nanodiscs reflects spontaneous binding of RNCs in absence of anionic lipids, such as DOPG. No interaction can be detected between nanodiscs and non-translating 70S ribosomes. Thus, the RNC binding is mainly mediated by the F_oc nascent chain, the hydrophobic domain of which likely partitioned spontaneously into the membrane. (B) The efficiency of the spontaneous YidC-independent insertion of F_oc into the membrane depends on the content of anionic lipids DOPG. Incorporation of YidC into nanodiscs will likely reduce the spontaneous insertion due to steric constraints at the membrane interface and the excluded volume within the lipid bilayer. FCS recordings were conducted in presence of 50 nM RNC F_oc-FL and the binding efficiency was calculated from the two-component model fitting.

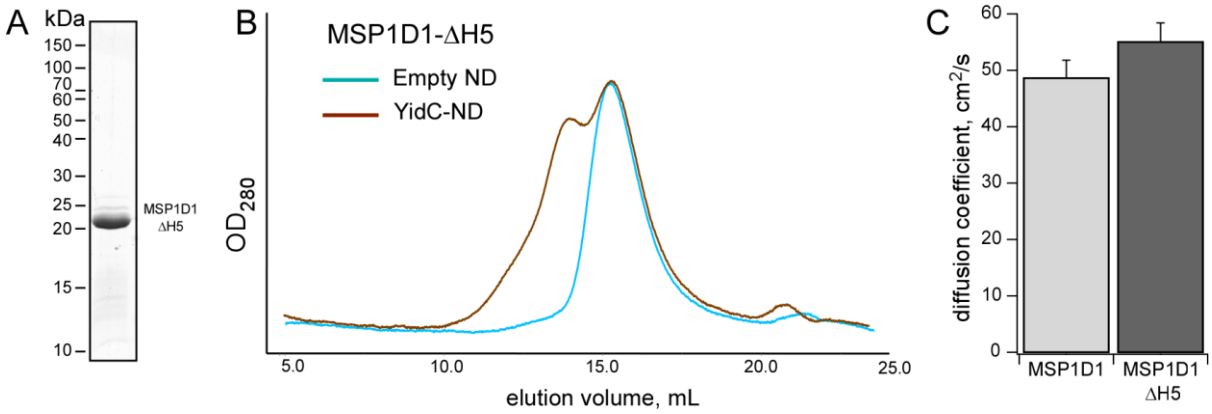

Figure S2. Related to the main text and Figure 4. Characterization of MSP1D1-ΔH5 nanodiscs. (A) SDS-PAGE of over-expressed and purified MSP1D1-ΔH5 variant. (B) Size-exclusion chromatography profile of empty and YidC-loaded nanodiscs formed by the MSP1D1-ΔH5 variant. (C) Lipid-loaded nanodiscs formed by the truncated MSP variant demonstrated higher diffusion coefficient than the original MSP1D1-based nanodiscs in agreement with the reduction in size (average diff. coef. + s.d.).

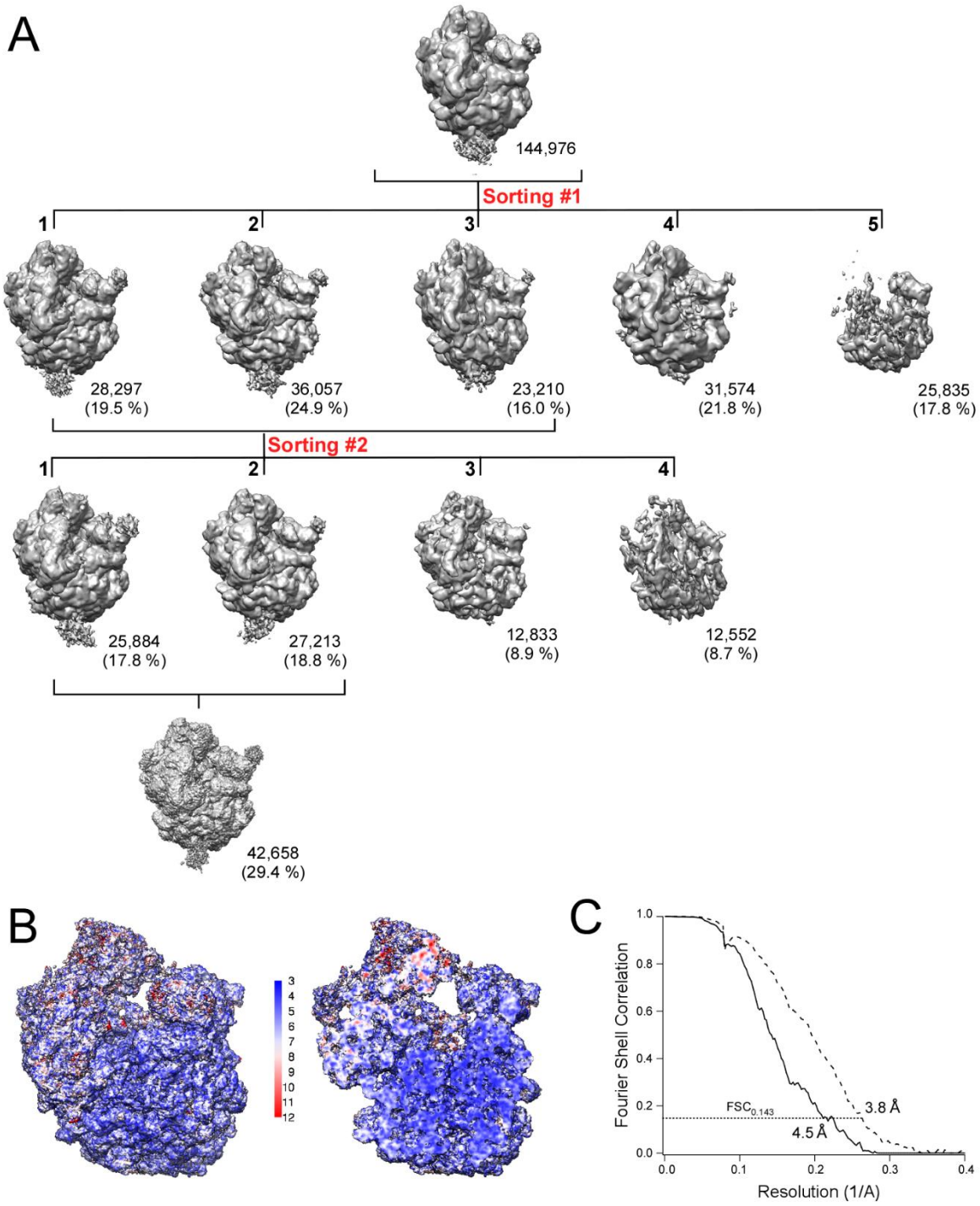

Figure S3. Related to Figure 5. Cryo-EM of the YidC-ND:RNC complex. (A) Sorting scheme of the cryo-EM data. The initial dataset of ribosomal particles displayed a strong density at the tunnel exit. FREALIGN-based sorting into 5 classes ("Sorting #1") allowed to separate partially dissociated ribosome (class 5) and ribosomes bound to other factors or occasional non-ribosomal particles (class 4). Classes 1 and 2 represented slightly different conformations of the ribosome, and class 3 demonstrated certain bias in orientation of particles. Classes 1-3 were merged and further sorted using a mask built of the large ribosomal subunit (50S) and a cylindrical density at the tunnel exit ("Sorting #2"). Dimensions of the masking cylinder exceeded the nanodisc approx. 2.5 fold. The sorting allowed

excluding particles with a strong orientation bias (class 4) and with a weak density for YidC-ND (class 3). Remaining classes 1 and 2 differed by an extension of YidC-ND, probably reflecting orientations of non-essential periplasmic P1 domain. These classes were merged and used for further refinement and modelling. The number of particles and its fraction in the initial data set (%) is indicated for each class. (B) Local resolution of the cryo-EM ribosome structure. Local resolution map of the surface (left) and interior (right) of the RNC F_oc-Δ10. The large ribosomal subunit (50S) was used for alignment of the dataset, resulting in a higher local resolution for the subunit. (C) FSC curves for 50S ribosomal subunit used for alignment (dashed line) and for the complex with YidC-ND (solid line). Corresponding average resolution values at $FSC_{0.143}$ are indicated.

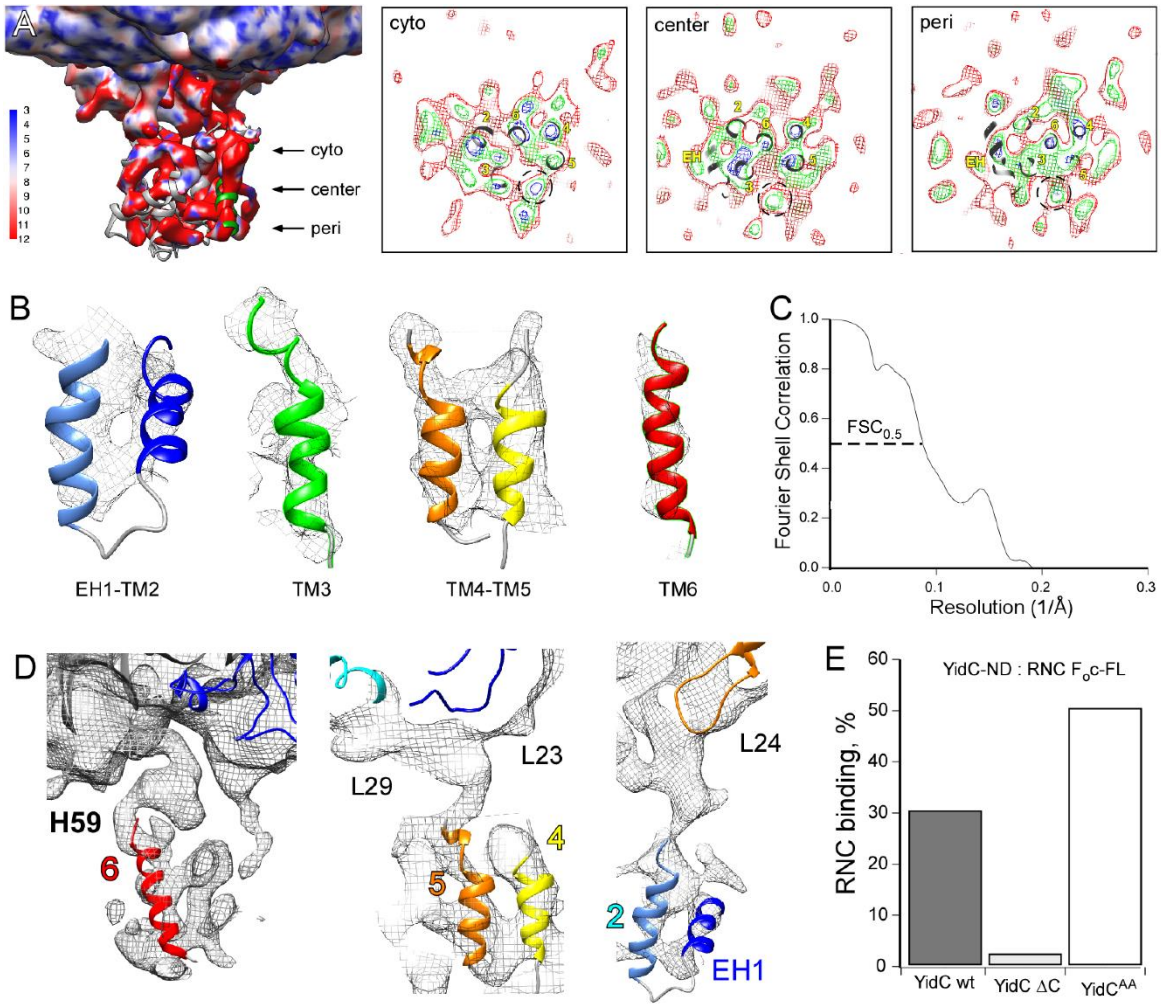

Figure S4. Related to Figure 5. Modelling the structure of YidC. (A) The local resolution map of YidC-ND reflects its higher flexibility compared to the ribosomal proteins. For modeling the YidC conformation its transmembrane helices were fitted in most prominent densities at the center of the nanodisc. Positioning of the helices within densities through the membrane plane at different levels (shown in blue/green/red) is shown on panels (right). (B) Fitting of YidC helices into cryo-EM densities. (C) FSC curve of model vs. map of nanodisc-embedded YidC. $FSC_{0.5}$ value of ~10 Å agrees with the limited local resolution of YidC-ND. (D) Primary contacts of YidC with the ribosome. The major contact site is built by C-terminal end of TM6 and the ribosomal RNA loop H59. Large density at the end of YidC TM6 may reflect the partially folded C-terminus. Short loop between YidC TM4 and TM5 approaches ribosomal protein L29 and L23. The pronounced extension near the ribosomal protein L24 likely reflects the position of YidC CH1-CH2 helical hairpin. (E) Mutations in the CH1-CH2 hairpin of YidC do not inhibit RNC binding. Nanodisc-reconstituted $YidC^{Y370A, Y377A}$ ($YidC^{AA}$) efficiently binds RNC F_oc-FL (50 nM) as tested by means of FCS.

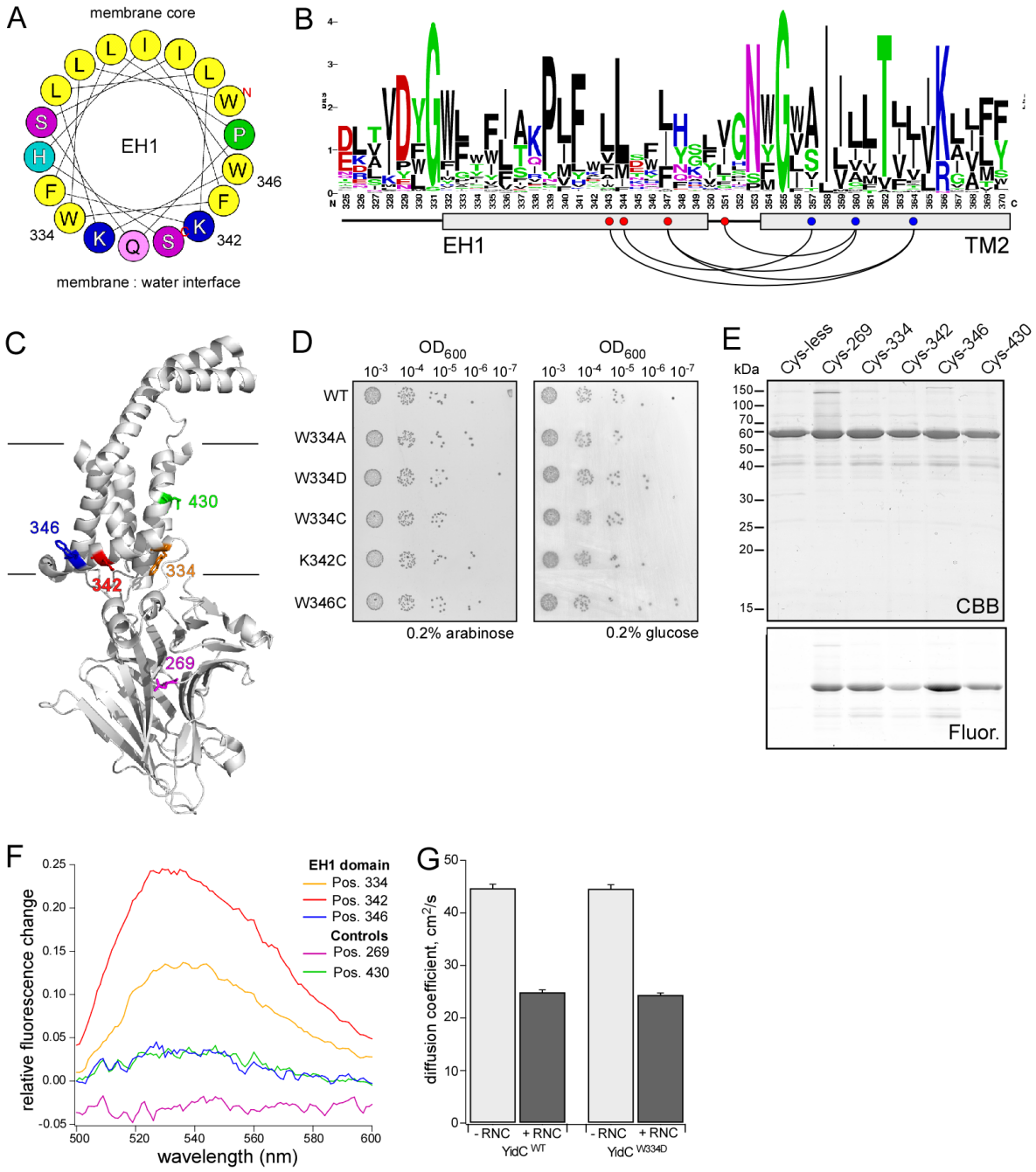

Figure S5. Related to Figure 6. Structural dynamics of the EH1 helix. (A) The wheel plot illustrates the amphipathic structure of the YidC EH1 helix, with a broad hydrophobic lipid-exposed interface (top), and a few polar/charged residues oriented towards the aqueous solvent (bottom). Positions of the IANBD fluorophore conjugated within EH1 are indicated. The wheel plot was generated using the HeliQuest server: http://heliquest.ipmc.cnrs.fr. (B) The sequence logo of the YidC EH1-TM2 region and evolutionarily coupled residues within. The sequence logo was generated using the WebLogo server: http://weblogo.berkeley.edu (C) Positions of the IANBD fluorophore conjugated to YidC are shown on the crystal structure of YidC in its idle state. (D) Point mutations within the EH1 helix do not affect the *in vivo* functionality of YidC. (E) Specificity of IANBD conjugation via the thioether bond was confirmed using a cysteine-less YidC variant as a negative control in the

labeling reaction. Occasional low-MW bands seen in SDS-PAGE likely originate from limited YidC degradation, as using cysteine-less YidC also prevented their labeling with IANBD. (F) Relative changes in IANBD fluorescence upon RNC F_oc-Δ5 binding depend on the fluorophore position. Variations in IANBD fluorescence levels between different positions within EH1 can be explained based on the structure of YidC: The transfer from the lipid head-group region to the acyl chains moiety upon ribosome binding should cause large changes in the polarity for the membrane interface-oriented residues 334 and 342. In contrast, the residue 346 is initially oriented towards the hydrophobic membrane core (A), and hence changes in the polarity and the associated IANBD fluorescence upon the EH1 displacement are substantially lower for this position. (G) An additional negative charge introduced into EH1 by mutation W334D does not affect RNC binding (diff. coef. + s.d.). The binding assay was performed by means of FCS using AlexaFluor 488-labeled $YidC^{D269C}$ variants in DPPG/DPPC-based nanodiscs and 150 nM RNC F_oc-FL.

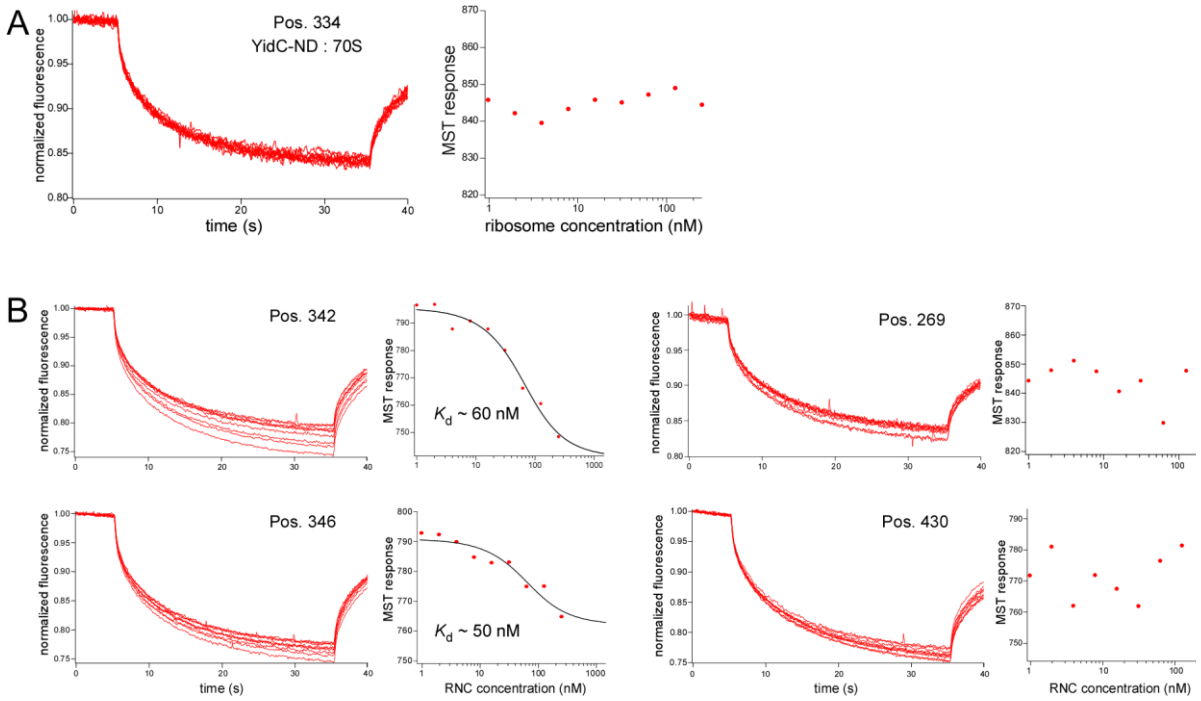

Figure S6. Related to Figure 6. Microscale thermophoresis on YidC^{IANBD}-ND: ribosome interactions. (A) The MST response of nanodisc-reconstituted YidC^{IANBD} is not affected by non-translating 70S ribosomes in agreement with the extremely low affinity. Left: normalized time-lapse fluorescence recordings; right: calculated fluorescence change, i.e. MST response upon local heating and thermal diffusion of fluorescently labeled YidC. (B) IANBD, an environment-sensitive dye conjugated within the EH1 helix (positions 342 and 346) allows resolving assembly of the YidC-ND:RNC complex, as the MST response is dependent on the RNC F_oc-Δ5 concentration. Notably, the MST response depended on the IANBD conjugation site within EH1, being the strongest for the position 342 and the weakest for 346 that correlates with IANBD fluorescence increase (Fig. 6). No interaction could be resolved when the dye is conjugated either at a solvent-exposed (position 269), or a statically buried within the membrane sites (position 430), that is likely due to a mutual compensation of several MST determinants, such as size and charge distribution.

Table S1. Related to Figure 6. Co-evolution of EH1-TM2 helices. A set of distanced residues in EH1 and TM2 form evolutionary conserved pairs within the YidC structure (highlighted in orange) and presumably build the interaction interface. Distances between Cβ atoms of those have been measured using the crystal structure of *E.coli* YidC (Kumazaki et al., 2014b). The co-evolution analysis data was adopted from David Baker's lab (http://gremlin.bakerlab.org/ecoli.php?uni=P25714), and residues separated by less than 6 positions in the primary sequence have been omitted from the table.

Res1	Res2	probability	distance, Å	new dist., Å	distance, aa
64	85	1			21
351	360	1	6.7	6.1	9
386	417	1			31
356	451	1			95
393	404	0.999			11
369	432	0.998			63
472	503	0.998			31
347	360	0.997	5.1	5.4	13
343	364	0.995	7.4	6.4	21
82	309	0.993			227
72	151	0.991			79
162	179	0.989			17
65	167	0.988			102
356	452	0.978			96
63	167	0.974			104
467	515	0.974			48
70	82	0.972			12
470	518	0.966			48
77	151	0.96			74
344	357	0.951	5.3	6.7	13
261	327	0.945			66
471	503	0.945			32
394	404	0.942			10
69	83	0.931			14
70	167	0.924			97
369	428	0.921			59
179	302	0.919			123
66	170	0.911			104
455	467	0.902			12
347	364	0.896	8.1	5.9	17
173	320	0.881			147
365	428	0.879			63
469	500	0.876			31